ARTICLE

Check for updates

Journal of
Sensor Science and Technology

The Korean Sensors Society

Development of Volumetric and Manometric Hydrogen Gas Sensors for Measuring Gas Emission and Diffusivity in H_2 Charged Polymers

Ji Hun Lee[1,+] and Sang Koo Jeon[1]

[1]*Hydrogen Energy Group, Korea Research Institute of Standards and Science, Daejeon 34113, Korea*

Cite This: *J. Sens. Sci. Technol. Vol. 34, No. 2 (2025) 76-88*

https://doi.org/10.46670/JSST.2025.34.2.76

ABSTRACT: Hydrogen gas sensors are important for industrial safety, environmental monitoring, and the gas industry. They detect hydrogen levels in the environment, ensuring safety and efficiency by providing accurate measurements. They are designed to be highly sensitive, stable, and reliable, and often require cost-effectiveness, fast response times, and compact designs. However, for certain purposes, high-performance H_2 gas sensors are required. Therefore, we developed two types of hydrogen gas sensors to meet these requirements. These sensors comprise volumetric and manometric types, which operate based on the principles of volume and pressure measurements, respectively. Measured values such as H_2 uptake, solubility, and diffusivity in H_2 gas-charged polymers in high-pressure environments were obtained using these gas sensors. The sensors respond instantly within one second and measure gas concentrations from 0.1 wt·ppm to 1500 wt·ppm with adjustable sensitivity, resolution, and measurement range. Performance tests of the two sensors confirmed their reliability, adjustable measurement range, and stability against temperature and pressure variations. As a result, this sensing system enabled real-time detection and characterization of gas transport properties for H_2 gas, making it suitable for high-pressure hydrogen gas applications.

KEYWORDS: *Volumetric measurement, Manometric measurement, Hydrogen, Uptake, Diffusivity, Polymer*

1. INTRODUCTION

Hydrogen is a clean and sustainable energy source [1-9] capable of replacing traditional fossil fuels and is gaining a critical position in the global renewable energy market because of its potential to reduce CO_x and NO_x emissions. However, hydrogen is highly explosive and flammable [10-21] when present at concentrations between 4% and 75% in air; thus, safety management is essential in the areas of production, transportation, and storage applications. For the measurement of hydrogen gas concentration and leakage, the H_2 gas sensor is normally employed. Therefore, the performance of the H_2 gas sensor for the immediate and sensitive detection of low concentrations of hydrogen to prevent leakage from hydrogen infrastructure has become a critical challenge in real-time gas-sensing technology.

Polymer materials play a significant role in hydrogen refueling stations charged with high-pressure H_2 [22-43]. In particular, polymer-based materials such as O-ring seals, gaskets, liner materials, and nonmetallic pipelines are widely used in hydrogen environments. However, these polymers are subjected to harsh conditions, including wide temperature and pressure fluctuations. These conditions can lead to seal damage, insufficient contact with the groove, and gas permeation through the polymer seals, all of which can result in hydrogen leakage [44-50].

Additional hydrogen leakage is caused by the degradation of polymer materials [45,51,52]. Seals and gaskets made of polymer materials used in hydrogen refueling stations are subjected to harsh conditions, including high and low temperatures and repeated pressure cycles. Over time, these materials degrade, weakening their physical properties and increasing their gas permeabilities, which can lead to long-term hydrogen leakage. This can undermine the safety of the hydrogen infrastructure and requires highly reliable real-time gas detection in polymer materials.

Therefore, hydrogen gas sensors are vital for accurately measuring hydrogen concentrations and leakage across applications where hydrogen is produced, stored, and used, such as fuel cells, storage facilities, and transportation systems [53,54].

[+]Corresponding author: ljh93@kriss.re.kr
Received : Feb. 3, 2025, Revised : Feb. 10, 2025, Accepted : Feb. 27, 2025

Hydrogen gas sensors rely on various sensing technologies that have unique advantages and limitations. Infrared (IR) sensing [55-63] measures hydrogen through its IR wavelength absorption properties, which are effective in specific environments but are often limited by their size, high cost, and power consumption, making them less suitable for compact and field-based applications. Semiconductor-based sensors [64-75] detect hydrogen by measuring changes in the resistance or conductivity on the sensor surface, which is often sensitive to temperature and humidity variations. These sensors may also respond to other gases, thereby posing selectivity challenges and potential long-term accuracy drifts. Catalytic combustion sensors [76-82] detect hydrogen by measuring the heat from hydrogen combustion on the catalyst surface. However, these sensors require oxygen for operation and lose sensitivity as the catalyst degrades, thereby limiting their use in oxygen-free or long-term applications. Optical spectroscopy [83-98] offers high-precision hydrogen detection in controlled laboratory settings. However, it is generally expensive, large, and requires frequent calibration, making it impractical for real-time or on-site applications.

Electrochemical hydrogen sensors [99-115] offer high sensitivity and selectivity, enabling the detection of low hydrogen concentrations. They are compact and energy-efficient, making them suitable for portable applications. However, these sensors can be influenced by factors such as temperature, pressure, and humidity. Periodic calibration may be required to maintain accuracy. Finally, gas chromatography [99,101,103,106,116-127] and mass spectrometry [128-140] provide highly precise analyses that are commonly used in research and laboratory settings. Mass spectrometry identifies gas molecules based on their mass after ionization, whereas gas chromatography separates and analyzes individual components in gas mixtures.

However, these sensing systems are expensive, require regular maintenance, and have a low processing speed. This renders them unsuitable for real-time field monitoring. In addition, conventional hydrogen gas-sensing technologies provide precise measurements but face challenges in terms of size, sensitivity, calibration, and environmental stability. These limitations highlight the need for advanced hydrogen sensors that are compact and exhibit rapid response times, high sensitivity, and robust performance across various field conditions to ensure safety in real-time hydrogen monitoring.

Thus, we developed two types of gas sensors with good performance. First, a sensor system for real-time hydrogen detection was proposed utilizing a volumetric measurement (VM) method based on an image-processing algorithm [5,141]. The system aims to provide real-time monitoring by connecting it to a computer via a GPIB interface and using a diffusion-permeation analysis program to accurately measure the H_2 concentration/diffusion with insensitivity to temperature and pressure changes.

Second, a simple H_2 sensor based on a manometric measurement (MM) method was developed using a portable USB-type data logger to measure and record the pressure/temperature in a sample container and a diffusion analysis program [142-144]. This portable detection system can easily measure the gas concentration/diffusion in a polymer specimen on-site in real time without any chemical reactions.

The developed H_2 sensor system is versatile for detecting and characterizing H_2 gas. It effectively measures the H_2 adsorption and diffusion in polymer materials in real time. The sensor exhibited reliable performance in terms of sensitivity, stability, and response time. The sensor technology presented in this study offers a compact, portable solution capable of replacing large-scale equipment with potential applications not only in hydrogen infrastructure safety management but also in the hydrogen gas industry for environmental monitoring.

The principles, procedures, results, and characteristics of each method were compared. Ultimately, these gas-sensing methods provide valuable insights into the H_2 transport properties, leakage, and sealing capabilities of rubber materials and O-rings under high-pressure conditions, which are applicable in H_2 fueling stations and H_2 infrastructure.

2. EXPERIMENTAL

2.1. Specimen Preparation and High-Pressure H_2 Gas Charging

The developed H_2 gas sensor was used to measure the H_2 gas concentration and diffusion coefficient of the polymer during the desorption process of the gas charged to high pressure. Polymers used include low-density polyethylene (LDPE), high-density polyethylene (HDPE), ethylene propylene diene monomer (EPDM), and nitrile butadiene rubber (NBR). LDPE and HDPE are widely used in the manufacture of containers and gas transport pipes. They exhibit gas-barrier properties when coated. EPDM and NBR were used as O-ring sealing materials in high-pressure gas tanks. The developed gas-detection system allowed us to investigate the permeation properties (solubility, diffusivity, and permeability) of the polymer samples.

LDPE and HDPE were manufactured by incorporating antimicrobial technology. The compositions and densities of the four polymer samples have been reported in previous studies [4,144]. EPDM and NBR were degassed by thermal treatment at 60°C for 48 h. The samples were prepared in the following cylindrical shapes and dimensions:

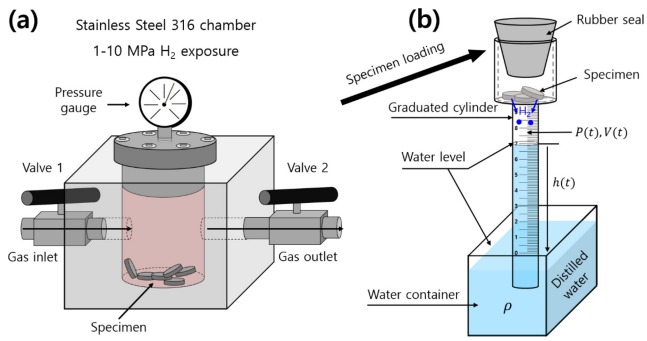

Fig. 1. Volumetric analysis system to measure the H_2 gas released by a specimen after exposure to high-pressure gas and decompression. (a) Specimen charged with gas in a high-pressure chamber. (b) After decompression in the chamber, the specimen was loaded into upper air space of graduated cylinder. The cylinder was immersed in a water container, and H_2 emission measurements were performed. Blue in cylinder represents water. The ● in the cylinder represents the H_2 gas emitted from charged sample.

- LDPE: radius (R) 9.51 mm, thickness (T) 4.89 mm
- HDPE: radius (R) 9.50 mm, thickness (T) 3.10 mm
- EPDM: radius (R) 9.51 mm, thickness (T) 2.53 mm
- NBR: radius (R) 9.51 mm, thickness (T) 2.18 mm

For high-pressure gas exposure, we used an SUS 316 chamber at room temperature under the desired pressure conditions. H_2 gas exposure was conducted at a pressure of 5 MPa. The purity of the H_2 gas was 99.999%.

The samples were charged with H_2 gas at a specified pressure for 24 h. A 24 h gas exposure was sufficient to reach equilibrium for H_2 sorption into the specimen. After the H_2 charging, the valve was opened to release H_2 gas from the chamber.

2.2. Volumetric Measurements for H_2 Concentration from Charged Polymers

A volumetric measurement technique to assess the hydrogen concentration and diffusion was developed. This method involves measuring the concentration of hydrogen released from a specimen after exposure to high pressures and decompression. Fig. 1 illustrates the volumetric analysis system used to quantify the hydrogen released at room temperature. The system consists of a chamber for hydrogen exposure and a graduated cylinder immersed in a water container.

After exposure to the high-pressure gas and decompression, the specimen was placed in the upper air space of the cylinder, as shown in Fig. 1. Hydrogen released from the specimen caused a gradual decrease in the water level within the cylinder. Consequently, the pressure (P) and volume (V) of the gas inside the cylinder varied with time.

The gas within the cylinder adheres to the ideal gas law, expressed as PV = nRT, where R is the gas constant (8.20544×10^{-5} m³·atm/(mol·K)), T represents the gas temperature inside the cylinder, and n denotes the number of moles of H_2 gas released into the cylinder. The variations in pressure P(t) and volume V(t) of the gas in the cylinder can be described as [145]

$$P(t) = P_o(t) - \rho g h(t),\ V(t) = V_o - V_s - V_h(t) \tag{1}$$

where P_o represents the external pressure surrounding the cylinder, g is the gravitational acceleration, and ρ signifies the density of distilled water. The $h(t)$ describes the water level within the graduated cylinder over time, and V_o is the combined volume of gas and water inside the cylinder measured relative to the water level in the container. $V_h(t)$ indicates the time-dependent volume of water in the cylinder, and V_s represents the volume occupied by the sample.

The amount of hydrogen gas released by the polymer specimen was quantified by tracking the water level position $[V_h(t)]$ over time. Consequently, the total number of moles of gas emitted $[n(t)]$ was calculated by measuring the total gas volume $[V(t)]$ in the cylinder, which corresponds to the decrease in the water level, as expressed by [145]

$$\begin{aligned} n(t) &= \frac{P(t)V(t)}{RT(t)} = \frac{P(t)[V_A+V_H(t)]}{RT(t)} = \frac{P_0[1+\beta(t)][V_A+V_H(t)]}{RT_0[1+\alpha(t)]} \\ &\cong \frac{P_0}{RT_0}\left[V_A + V_H(t) + V(t)\left(\beta(t)-\alpha(t)\right)\right] \\ &= n_A(t) + n_H(t), \\ \text{with } n_A(t) &= \frac{P_0}{RT_0}V_A, \\ n_H(t) &= \frac{P_0}{RT_0}[V_H(t) + V(t)(\beta(t)-\alpha(t))] \\ \alpha(t) &= \frac{T(t)-T_0}{T_0},\ \ \beta(t) = \frac{P(t)-P_0}{P_0} \end{aligned} \tag{2}$$

where T_0 represents the initial temperature of H_2 in the cylinder, and P_0 is the pressure of H_2 in the cylinder. $V(t)$ is the total volume consisting of the remaining initial air volume (V_A) and the released H_2 volume $[V_H(t)]$, such that $V(t) = V_A + V_H(t)$. n_A denotes the initial mole number of air, and $n_H(t)$ refers to the time-dependent mole number of H_2 corresponding to the increase in hydrogen volume due to its release. Therefore, $n_H(t)$ was converted into the hydrogen concentration, $[C(t)]$ emitted per unit mass from the specimen as follows:

$$\begin{aligned} &C(\mathrm{t})[\mathrm{wt}\cdot\mathrm{ppm}] \\ &= n_H(t)[\mathrm{mol}] \times \frac{m_{H2}\left[\frac{\mathrm{g}}{\mathrm{mol}}\right]}{m_{sample}[\mathrm{g}]} \times 10^6 \\ &= \frac{P_0}{RT_0}[V_H(t) + V(t)(\beta(t)-\alpha(t))][\mathrm{mol}] \times \frac{m_{H2}\left[\frac{\mathrm{g}}{\mathrm{mol}}\right]}{m_{sample}[\mathrm{g}]} \times 10^6 \end{aligned} \tag{3}$$

The molar mass of hydrogen gas, m_{H2} [g/mol], was 2.016 g/mol, and m_{sample} is the specimen mass. In Eqs. (2) and (3),

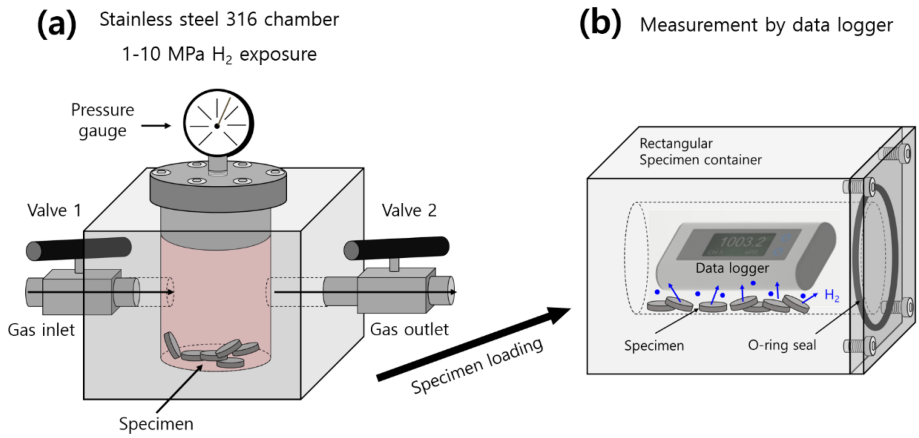

Fig. 2. Schematic of manometric analysis system used to measure H_2 gas uptake and diffusivity in charged sample, utilizing a commercial pressure/temperature logger after high-pressure exposure and decompression. (a) The sample is charged with gas inside the high-pressure chamber. (b) After decompression, the charged sample is loaded in a rectangular specimen container. H_2 gas emission is then measured using a data logger in the container. The ● in the specimen container represents the H_2 gas emitted from charged sample.

the time-dependent mole number of H_2, $n_H(t)$, was converted into the H_2 mass concentration, $[C(t)]$, using the factor $k=\left[\frac{m_{H_2}}{m_{sample}}\right]$. $n_H(t)$ and $C(t)$ are affected by fluctuations in the temperature and pressure in laboratory environments. To ensure precise measurement, it is essential to compensate for these variations. This compensation can be achieved through automated programs according to Eq. (3). That is., the term $V(t)(\beta(t)-\alpha(t))$ indicates the volume change in $V_H(t)$, caused by the temperature and pressure variations. The compensation indicates the application of $V(t)(\beta(t)-\alpha(t))$ calculation in Eq. (3). Thus, the insensitivity of the sensor to variations in temperature and pressure indicated the application of automatic compensation by the program.

The release of hydrogen gas was tracked by monitoring changes in the water level using an image-processing algorithm or digital camera.

2.3. Pressure Measurement for H_2 Concentration from Charged Polymers

Fig. 2 shows a schematic of the manometric measurement system used to determine the concentration and diffusivity of the hydrogen gas released from the specimen at room temperature. The setup included a high-pressure chamber for H_2 gas exposure, as shown in Fig. 2 (a), and a rectangular specimen container equipped with a USB-type data logger and rubber seal, as shown in Fig. 2 (b). The ELP sensors used to measure the pressure and temperature are commercial data loggers capable of simultaneously recording atmospheric pressure and temperature.

After exposure and decompression in the high-pressure chamber, the specimen was transferred to a rectangular container, as shown in Fig. 3 (b). As the hydrogen gas was emitted from the sample, the pressure inside the vessel increased over time. Consequently, both the pressure (P) and temperature (T) of the gas within the specimen container changed over time. The hydrogen gas inside the container followed the ideal gas law: $PV = nRT$, where R is the gas constant with 8.20544×10^{-5} m³ ·atm/(mol·K), and n represents the number of moles of the released gas molecules inside the specimen container.

The number of moles of gas emitted from the charged specimen was obtained by measuring the increase in pressure $[P(t)]$ versus time using manometric measurements at a constant container volume. Thus, the total number of moles $[n(t)]$ obtained by measuring the increased gas pressure $[P(t)]$ due to the gas emitted in the cylindrical container is described as follows [4,144]:

$$\begin{aligned} n(t) &= \frac{P(t)V_0}{RT(t)} = \frac{P(t)V_0}{RT(t)} = \frac{[P_0+\Delta P(t)]V_0}{RT_0[1+\alpha(t)]} \\ &\cong \frac{P_0V_0+\Delta P(t)V_0}{RT_0}[1-\alpha(t)] = n_0 + \Delta n(t), \\ &\text{with } n_0 = \frac{P_0V_0}{RT_0},\ \Delta n(t) = \frac{V_0}{RT_0}[\Delta P(t) - \alpha(t)P_0 - \\ &\alpha(t)\Delta P(t)] \\ &\alpha(t) = \frac{T(t)-T_0}{T_0} \end{aligned} \quad (4)$$

where T_0, V_0 and P_0 are the temperature, initial volume, and initial pressure of the air, respectively, at the initial time inside the cylinder. $P(t)$ is the sum of remaining initial air pressure (P_o) and time-varying released gas pressure $[\Delta P(t)]$ from specimen, i.e., $P(t) = P_o + \Delta P(t)$, n_0 is remaining initial air mole, and $\Delta n(t)$ is the time-varying gas mole corresponding to gas pressure increase from the released gas. $\alpha(t)$ is the change rate of temperature with respect to T_0. Thus, $\Delta n(t)$ is transformed into the released gas concentration $[\Delta C(t)]$ per mass for specimen as [144]:

$$\Delta C(\mathrm{t})[\mathrm{wt}\cdot\mathrm{ppm}] = \Delta n(t)[\mathrm{mol}] \times \frac{m_g\left[\frac{\mathrm{g}}{\mathrm{mol}}\right]}{m_{specimen}[\mathrm{g}]} = \frac{V_0}{RT_0}[\Delta P(t) - \alpha(t)P_0 - \alpha(t)\Delta P(t)][\mathrm{mol}] \times \frac{m_g\left[\frac{\mathrm{g}}{\mathrm{mol}}\right]}{m_{specimen}[\mathrm{g}]} \times 10^6 \quad (5)$$

where m_g [g/mol] is the molar mass of the hydrogen gas used; for H_2, m_{H2} [g/mol] = 2.016 g/mol and $m_{specimen}$ is the sample mass. The first term, $\Delta P(t)$ in Eq. (5), is the increase in pressure emitted by the gas from the sample. The second term, $-\alpha(t)P_0$, is the pressure change caused by temperature variation $[\alpha(t)]$. The third term, $-\alpha(t)\Delta P(t)$ is the pressure change due to both temperature variation $[\alpha(t)]$ and pressure increase $[\Delta P(t)]$.

According to Eqs. (4) and (5), the time-varying hydrogen gas mole, $\Delta n(t)$, is transformed to hydrogen gas mass concentration, $[[\Delta C(t)]$, by $k = \left[\frac{m_g}{m_{specimen}}\right]$. $\Delta n(t)$ and $\Delta C(t)$ are affected by both temperature and pressure variations. Thus, we compensated for the variations caused by the changes in temperature and pressure.

2.4. Analysis Program for Obtaining Transport Parameters

Assuming that hydrogen gas emission from the gas-charged sample follows Fickian diffusion, the concentration of the released gas, $C_E(t)$, is calculated as [146,147]:

$$C_E(t)/C_\infty = 1 - \frac{32}{\pi^2} \times \left[\sum_{n=0}^{\infty} \frac{\exp\left\{\frac{-(2n+1)^2\pi^2 Dt}{l^2}\right\}}{(2n+1)^2}\right] \times \left[\sum_{n=1}^{\infty} \frac{\exp\left\{-\frac{D\beta_n^2 t}{\rho^2}\right\}}{\beta_n^2}\right]$$
$$= 1 - \frac{32}{\pi^2} \times \left[\frac{\exp\left(-\frac{\pi^2 Dt}{l^2}\right)}{1^2} + \frac{\exp\left(-\frac{3^2\pi^2 Dt}{l^2}\right)}{3^2} + \cdots, + \frac{\exp\left(-\frac{(2n+1)^2\pi^2 Dt}{l^2}\right)}{(2n+1)^2} + \cdots,\right] \quad (6)$$
$$\times \left[\frac{\exp\left(-\frac{D\beta_1^2 t}{\rho^2}\right)}{\beta_1^2} + \frac{\exp\left(-\frac{D\beta_2^2 t}{\rho^2}\right)}{\beta_2^2} + \cdots, + \frac{\exp\left(-\frac{D\beta_n^2 t}{\rho^2}\right)}{\beta_n^2} + \cdots,\right]$$

where β_n represents the root of the zeroth-order Bessel function $J_0(\beta_n)$. Eq. (6) is the solution to Fick's second diffusion equation for a cylindrical specimen. $C_E(t = 0) = 0$ and $C_E(t = \infty) = C_\infty$ is saturated hydrogen gas concentration at infinite time (gas uptake). D is gas diffusivity. l and ρ are thickness and radius of cylindrical sample, respectively.

Many of the terms in the two summations of Eq. (6) are included. Thus, an analysis program was developed to accurately calculate C_∞ and D. Using an analysis program based on an optimization algorithm [135,148], we accurately calculate $C_E(t)$ and D from the measured results by solving Eq. (6).

3. RESULTS AND DISCUSSIONS

3.1. Volumetric Measurement

After decompressing a specimen enriched with hydrogen under high pressure, the water level in the VM method was measured using an image-processing algorithm and a digital camera [141]. According to Eqs. (3) and (6), the concentration and diffusivity of the released hydrogen gas were determined using the VM method with a graduated cylinder (Fig. 1). Figs. 3 (a)–(d) illustrate the H_2 gas volume (blue filled circle) transferred from the water level measurement and hydrogen emission content (black open square) in units of wt·ppm for cylindrical LDPE, HDPE, EPDM, and NBR specimens. The right side of Figs. 3 (a) through (d) represents the diffusion parameters, D and C_∞, derived using an analysis program by Eq. (6). The blue lines in Figs. 3 (a) through (d) represent the fitted values obtained using Eq. (6), with the H_2 diffusivity and total hydrogen uptake marked by a blue arrow.

3.2. Manometric Measurement

After decompressing the specimens enriched with hydrogen under high pressure, the released H_2 gas concentration and diffusivity were determined using the MM method for the specimens loaded in a cylindrical container (Fig. 2). According to Eq. (5), the H_2 gas concentration in the MM method was obtained from the temperature/pressure using a commercial USB-type manometer. Similar to Fig. 3, Figs. 4 (a) through (d), the H_2 gas volume (blue filled circle) was transferred from the measured pressure and hydrogen emission content (black open square) in units of wt·ppm for the cylindrical LDPE, HDPE, EPDM, and NBR specimens. The right side of Figs. 4 (a) through (d) represents the diffusion parameters, D and, C_∞ derived using an analysis program by Eq. (6). The blue lines in Figs. 4 (a) through (d) represent the values fitted using Eq. (6), with the H_2 diffusivity and total hydrogen uptake marked by a blue arrow.

As shown in Figs. 3 and 4, single-mode hydrogen emission behaviors in LDPE, HDPE, EPDM, and NBR were observed in time-varying hydrogen emission measurements. The single-mode hydrogen emission in all specimens investigated in this study was attributed to gas diffusion into the amorphous phase.

Moreover, the solubility S is obtained from the H_2 uptake versus pressure plot in Figs. 3 and 4 as follows [142,149-151]:

$$S\left[\frac{mol}{m^3 \cdot MPa}\right] = \frac{(C_\infty/\mathrm{pressure})\left[\frac{wt\cdot ppm}{MPa}\right] \times 10^6 \times d\left[\frac{g}{m^3}\right]}{m_g\left[\frac{g}{mol}\right]} \quad (7)$$

m_g is the molar mass of H_2 gas (2.016 g/mol), and d is the sample density. The solubilities and diffusivities of the two sensors for H_2 gas in the LDPE, HDPE, EPDM, and NBR samples are listed in Table 1.

As shown in Table 1, the solubility and diffusivity in the four specimens for the two sensors exhibited a 10% relative expanded uncertainty for the measured value. The solubility

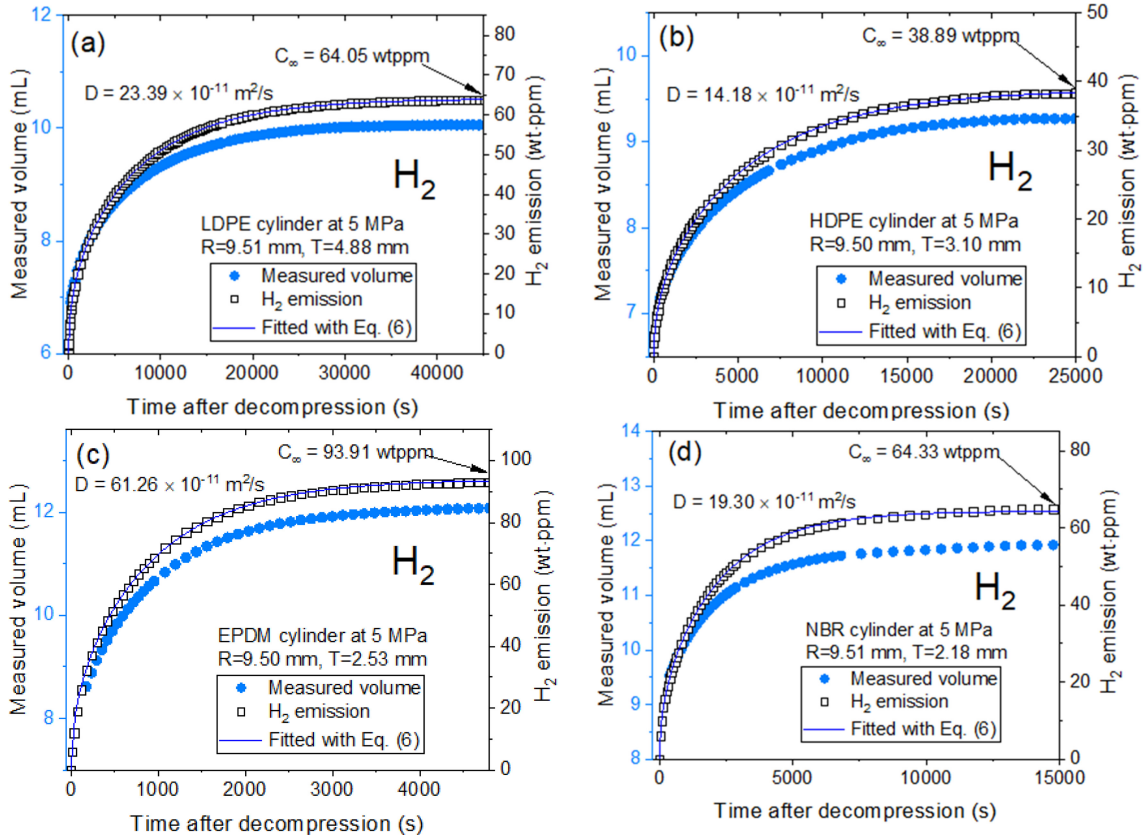

Fig. 3. Diffusion parameters determined in cylindrical LDPE, HDPE, EPDM, and NBR specimen using volumetric method with image-processing algorithm and a digital camera. (a-d): Measured volume (blue filled circle) converted from the measured water level and H_2 emission (black open square) derived from the measured H_2 volume in units of wt·ppm for four specimens. The difference in patterns between the measured volume and H_2 emission is due to temperature/pressure compensation applied using Eq. (2). The blue line represents the fitted results by Eq. (6), with gas diffusivity (D) and the total gas uptake (C_∞) indicated by a blue arrow. Here, R is the radius and T is the thickness of the cylindrical specimen.

and diffusivity results determined from both VM and MM were consistent with the estimated relative uncertainty.

3.3. Performance Comparison between Volumetric and Manometric Gas Sensors

We evaluated the performances of the two H_2 gas-sensing systems using a manometric data logger sensor and a volumetric image sensor. The results of the performance tests, including sensitivity, resolution, stability, measurable range, response time, and figure of merit are presented in Table 2. The sensitivity of the volumetric and manometric sensors is defined as the change in mass concentration relative to the change in volume and pressure, respectively. The obtained sensitivities were 16.43 wt·ppm/mL for the volumetric sensor and 11.96 wt·ppm/hPa for the manometric sensor. A sensor with a higher sensitivity typically provides better resolution. The resolution of the volumetric sensor was reflected by a minimum measurable volume of 0.005 mL, which corresponded to a mass concentration of 0.08 wt·ppm. The resolution of the manometric sensor was reflected by the minimum measurable pressure (0.01 hPa), corresponding to a mass concentration of 0.12 wt·ppm. To further improve the resolution, it is possible to reduce the inner volume of the graduated cylinder and sample container or increase the number of specimens. This adjustment leads to better sensitivity and resolution.

The stability of the two sensor systems was quantified by the standard deviation of measurements taken over 36 h after gas emission from the specimen ceased. This was less than 0.2% of the mass concentration for both sensors. The measurable range was defined as the maximum allowable concentration per specimen weight within a container with an inner volume. For both sensors, the measurable range was less than 1500 wt·ppm, which can be adjusted by varying the sample weight and specimen container volume. The volume and pressure responses of the gas sensor are almost instantaneous, occurring within 1 s of gas emission. The FOM is defined as the standard deviation between the measured data and theoretical value calculated using Eq. (3). An FOM value below 0.4% for the volumetric sensor and 0.7% for the manometric sensor indicated

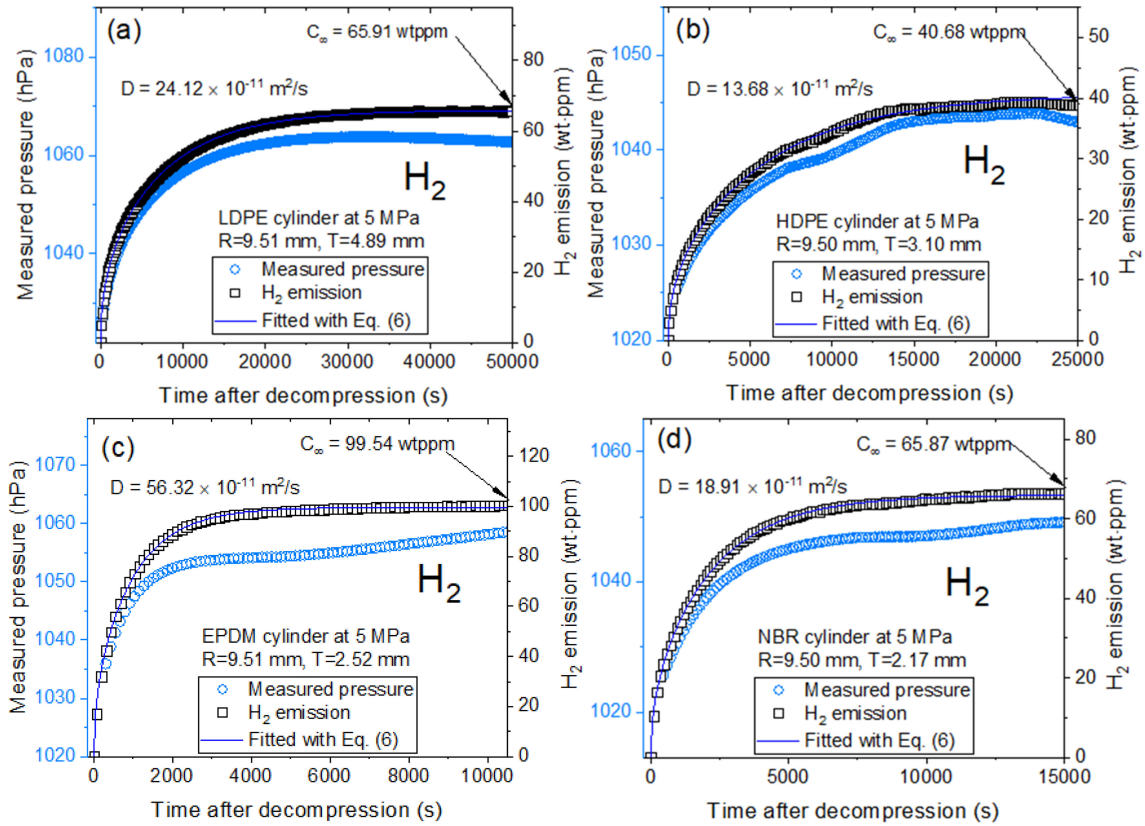

Fig. 4. Diffusion parameters determined in cylindrical LDPE, HDPE, EPDM, and NBR specimens by manometric method using USB-type manometer and specimen container. (a-d): Measured pressure (blue filled circle) and H_2 emission (black open square) transferred from measured H_2 pressure in units of wt·ppm for four specimens. The difference in patterns between the measured pressure and H_2 emission is due to temperature/pressure compensation applied using Eq. (4). The blue line represents the fitted results by Eq. (6), with gas diffusivity (D) and the total gas uptake (C_∞) marked by a blue arrow. Here, R is the radius and T is the thickness of the cylindrical specimen.

Table 1. Solubility and diffusivity of hydrogen gas determined in four different polymers.

Method	Solubility [mol/m^3·MPa]				Diffusivity [$\times 10^{-11}$ m^2/s]			
	LDPE	HDPE	EPDM	NBR	LDPE	HDPE	EPDM	NBR
VM	5.83	3.67	10.15	7.79	23.39	14.18	61.26	19.30
MM	6.00	3.83	10.76	7.97	24.12	13.68	56.32	18.91

Table 2. Performance comparisons for two sensor systems using volumetric and manometric methods

Performance	Volumetric measurement	Manometric measurement
Sensitivity	16.43 wt·ppm/mL	11.96 wt·ppm/hPa
Resolution	0.08 wt·ppm	0.12 wt·ppm
Stability	≤ 0.2%	≤ 0.2%
Measuring range	Max. 1400 wt·ppm	Max. 1500 wt·ppm
Response time	≤ 1 s	≤ 1 s
FOM	0.4%	0.7%

good agreement between the theoretical and measured values. Based on performance testing, the specifications (sensitivity, resolution, and FOM) of the VM sensor were superior to those of the MM sensor.

4. CONCLUSIONS

Hydrogen gas sensors are important for ensuring the safety and protection of hydrogen infrastructure. To meet these requirements, we developed two hydrogen-sensing systems that utilize volumetric measurements with a graduated cylinder, image-processing algorithm, and digital camera. Changes in the pixel position of the water level in the cylinder due to the released hydrogen were correlated with the emitted H_2 gas volume, enabling precise H_2 content measurements. By incorporating a diffusion-permeation analysis program, this

volumetric image hydrogen sensor can effectively detect H_2 concentrations and diffusivity from H_2-enriched specimens under high-pressure conditions.

A simple manometric gas-sensing system was developed to characterize hydrogen gas. This technique, based on pressure measurements in a gas-charged specimen container and using a simple commercial data logger, leveraged the increase in gas pressure caused by H_2 gas released from high-pressure polymer specimens to determine the H_2 gas concentration and diffusivity via a diffusion analysis program.

The two effective and portable hydrogen sensor systems demonstrated several performance metrics: a low detection limit of H_2 content, a measurable range of up to 1500 wt·ppm, stability of 0.2%, and a rapid response time within 1 s. Furthermore, the insensitivity of the two sensors to temperature and pressure fluctuations makes them suitable for gas detection. High-performance systems with volumetric and manometric methods demonstrated successful real-time measurement and characterization of H_2. They effectively measure the uptake and diffusivity of gases emitted from specimens with expanded uncertainty by considering the influencing factors. The main features of the two developed gas-sensing methods are as follows.

- **Cost-effective and simple techniques:** These two methods offer inexpensive and straightforward approaches for measuring the gas uptake and diffusivity in H_2-charged polymers.
- **Stability with respect to temperature and pressure:** The two methods are stable against variations in temperature and pressure and are suitable for diverse specimen sizes and shapes.
- **Precise calculation:** Each method enables exact calculation by an analysis program.
- **Adjustable sensitivity and range:** Volumetric and manometric methods allow for adjustable sensitivity, resolution, and measurement range.
- **Visible H_2 release monitoring:** The volumetric method offers visual monitoring of gas release and leakage through changes in the water level.

The solubility and diffusivity results obtained from both the volumetric and manometric measurements were consistent with the estimated relative uncertainty. These two complementary methods are well suited for effectively measuring the hydrogen gas transport properties in sealing elastomers and can be applied to evaluate the permeation characteristics of rubber materials and O-rings under high-pressure conditions, making them ideal for use in hydrogen fueling station applications.

Authorship Contribution Statement

Ji Hun Lee: Conceptualization, Investigation, Methodology, Validation, Writing - original draft, Writing - review & editing. **Sang Koo Jeon:** Methodology.

Declaration of Competing Interest

The authors declare that they have no known competing financial interests or personal relationships that could have appeared to influence the work reported in this paper.

Acknowledgements

This research was supported by the Development of Reliability Measurement Technology for Hydrogen Fueling Stations funded by the Korea Research Institute of Standards and Science (KRISS-2025-GP2025-0014)

REFERENCES

[1] V.V. Patil, A.S.N. Husainy, K. Shedbalkar, S.N. Momin, O.S. Chougule, P.U. Jadhav, S.S. Shinde, P. Singh, Review on revolutionary and sustainable green hydrogen: A future energy source, In: A. K. Agarwal (Eds.), Energy, Environment, and Sustainability, Springer, Singapore, 2024 pp. 39–54.
[2] M. Yoshida, More than clean, sustainable, and renewable energy source: New therapeutic role for hydrogen?, JACC Basic Transl. Sci. 7 (2022) 162–163.
[3] S.E. Hosseini, M. A. Wahid, Hydrogen from solar energy, a clean energy carrier from a sustainable source of energy, Int. J. Energy Res. 44 (2020) 4110–4131.
[4] J.K. Jung, I.G. Kim, K.S. Chung, U.B. Baek, Analyses of permeation characteristics of hydrogen in nitrile butadiene rubber using gas chromatography, Mater. Chem. Phys. 267 (2021) 124653.
[5] J.K. Jung, J.H. Lee, High-performance hydrogen gas sensor system based on transparent coaxial cylinder capacitive electrodes and a volumetric analysis technique, Sci. Rep. 14 (2024) 1967.
[6] F. Qureshi, M. Asif, A. Khan, H. Aldawsari, M. Yusuf, M.Y. Khan, Green hydrogen production from non-traditional water sources: a sustainable energy solution with hydrogen storage and distribution, Chem. Rec. 24 (2024) e202400080.
[7] I. Requena-Leal, C.M. Fernández-Marchante, J. Lobato, M.A. Rodrigo, Towards a more sustainable hydrogen energy production: Evaluating the use of different sources of water for chloralkaline electrolyzers, Renew. Energy 233 (2024) 121137.
[8] S.U. Batgi, I. Dincer, Design of a two-renewable energy source-based system with thermal energy storage and hydrogen storage for sustainable development, J. Energy Storage 89 (2024) 111742.
[9] R. Liu, Y.A. Solangi, An analysis of renewable energy sources for developing a sustainable and low-carbon hydrogen economy in China, Processes 11 (2023) 1225.
[10] H.M. Kang, M.C. Choi, J.H. Lee, Y.M. Yun, J.S. Jang, N.K.

Chung, et al., Effect of the high-pressure hydrogen gas exposure in the silica-filled EPDM sealing composites with different silica content, Polymers 14 (2022) 1151.
[11] R. Sun, L. Pu, H. Yu, M. Dai, Y. Li, Modeling the diffusion of flammable hydrogen cloud under different liquid hydrogen leakage conditions in a hydrogen refueling station, Int. J. Hydrog. Energy 47 (2022) 25849–25863.
[12] I. Amez, B. Castells, D. León, R. Paredes, Study of quaternary hydrogen and biogas mixtures: An industrial safety approach, Fuel 381 (2025) 133663.
[13] M. Wu, L. Bai, F. Deng, J. He, K. Song, H. Li, Organic-inorganic hybrid materials for catalytic transfer hydrogenation of biomass-derived carbonyl-containing compounds, Coord. Chem. Rev. 523 (2025) 216259.
[14] M. Tang, C. Qin, X. Sun, M. Li, Y. Wang, J. Cao, Y. Wang, Enhanced H2 gas sensing performances by Pd-loaded In2O3 microspheres, Appl. Phys. A 130 (2024) 741.
[15] H. Jia, Z. An, B. Qi, G. Yang, X. Ma, A study on the effect of air humidity on jet flames of hydrogen ships, E3S Web Conf. 561 (2024) 01012.
[16] A. Tom, D.K. Singh, V.K. Shaw, P.V. Abhijith, S. Sajana, P.S. Kirandas, et al., Jaiswal-Nagar, Feedback based gas sensing setup for ppb to ppm level sensing, Rev. Sci. Instrum. 95 (2024) 085003.
[17] R. Venkatesan, R. Harun, H.M. Yusoff, M.A. Razak, Hydrogen safety effect calculation (dispersion and thermal radiation effects) for determination of siting and safe distance, Process Saf. Prog. 43 (2024) S161–S169.
[18] A.A. Malik, R. Rusli, S. Nazir, R.H. Wong, U. Arshad, Grid-based assessment of hydrogen leakages for an offshore process to improve the design and human performance, Process Saf. Prog. 43 (2024) S35–S49.
[19] J.N. Lu, Y. Huang, Y.S. Xia, L.Z. Dong, L. Zhang, J.J. Liu, et al., Selective photosynthesis of Z-olefins through crystalline metal–organic cage-initiated expeditious cascade reactions, Carbon Energy 6 (2023) e396.
[20] R. B. Gupta, Hydrogen sensing and detection, in Hydrogen Fuel: Production, Transport, and Storage, CRC Press, Boca Raton, 2008.
[21] W.J. Buttner, M.B. Post, R. Burgess, C. Rivkin, An overview of hydrogen safety sensors and requirements, Int. J. Hydrog. Energy 36 (2011) 2462–2470.
[22] Y. Wang, Y. Pang, H. Xu, A. Martinez, K.S. Chen, PEM Fuel cell and electrolysis cell technologies and hydrogen infrastructure development–a review, Energy Environ. Sci. 15 (2022) 2288–2328.
[23] Y. Wang, B. Seo, B. Wang, N. Zamel, K. Jiao, X.C. Adroher, Fundamentals, materials, and machine learning of polymer electrolyte membrane fuel cell technology, Energy AI 1 (2020) 100014.
[24] E.R. Duranty, T.J. Roosendaal, S.G. Pitman, J.C. Tucker, S.L. Owsley, J.D. Suter, K.J. Alvine, An in situ tribometer for measuring friction and wear of polymers in a high pressure hydrogen environment, Rev. Sci. Instrum. 88 (2017) 095114.
[25] H.M. Kang, J.W. Bae, J.H. Lee, Y.M. Yun, S.K. Jeon, N. K. Chung, et al., The Synergistic Effect of Carbon Black/Carbon Nanotube Hybrid Fillers on the Physical and Mechanical Properties of EPDM Composites after Exposure to High-Pressure Hydrogen Gas, Polymers 16 (2024) 1065.
[26] B.L. Choi, J.K. Jung, U.B. Baek, B.H. Choi, Effect of functional fillers on tribological characteristics of acrylonitrile butadiene rubber after high-pressure hydrogen exposures, Polymers 14 (2022) 861.
[27] I. Profatilova, F. Fouda-Onana, M. Heitzmann, T. Bacquart, A. Morris, J. Warren, et al., Detrimental impact of trace amount of tetrachlorohexafluorobutane impurity in hydrogen on PEM fuel cell performance, Int. J. Hydrog. Energy 65 (2024) 837–843.
[28] N. Kopacak, H.C. Güldorum, O. Erdinc, Implementation of a decision-making approach for a hydrogen-based multi-energy system considering EVs and FCEVs availability, IEEE Access 12 (2024) 114705–114721.
[29] S.U. Zhanguo, W. Zhang, A. Abdulwahab, S. Saleem, Y. Yao, A. Deifalla, et al., Comparison of gasoline and hydrogen pathways in order to reduce the environmental hazards of a solar-hydrogen refueling station: Evaluation based on life cycle cost and Well-To-Wheel models, Process Saf. Environ. Prot. 173 (2023) 317–331.
[30] J.K. Jung, U.B. Baek, S.H. Lee, M.C. Choi, J.W. Bae, Hydrogen gas permeation in peroxide-crosslinked ethylene propylene diene monomer polymer composites with carbon black and silica fillers, J. Polym. Sci. 61 (2023) 460–471.
[31] J.K. Jung, J.H. Lee, S.K. Jeon, U.B. Baek, S.H. Lee, C.H. Lee, et al., H_2 uptake and diffusion characteristics in sulfur-crosslinked ethylene propylene diene monomer polymer composites with carbon black and silica fillers after high-pressure hydrogen exposure reaching 90 MPa, Polymers 15 (2023) 162.
[32] D. Pivetta, C. Dall'Armi, R. Taccani, Multi-objective optimization of a hydrogen hub for the decarbonization of a port industrial area, J. Mar. Sci. Eng. 10 (2022) 231.
[33] S. Toghyani, E. Baniasadi, E. Afshari, Performance assessment of an electrochemical hydrogen production and storage system for solar hydrogen refueling station, Int. J. Hydrog. Energy 46 (2021) 24271–24285.
[34] B. Flamm, C. Peter, F.N. Büchi, J. Lygeros, Electrolyzer modeling and real-time control for optimized production of hydrogen gas, Appl. Energy 281 (2021) 116031.
[35] W. Kuang, W.D. Bennett, T.J. Roosendaal, B.W. Arey, A. Dohnalkova, G. Petrossian, et al., In situ friction and wear behavior of rubber materials incorporating various fillers and/or a plasticizer in high-pressure hydrogen, Tribol. Int. 153 (2021) 106627.
[36] J.H. Lee, Y.W. Kim, D.J. Kim, N.K. Chung, J.K. Jung, Comparison of two methods for measuring the temperature dependence of H_2 permeation parameters in nitrile butadiene rubber polymer composites blended with fillers: The volumetric analysis method and the differential pressure method, Polymers 16 (2024) 280.
[37] J.H. Lee, Y.W. Kim, J.K. Jung, Investigation of the gas permeation properties using the volumetric analysis technique for polyethylene materials enriched with pure gases under high pressure: H_2, He, N_2, O_2 and Ar, Polymers 15 (2023) 4019.
[38] J.K. Jung, J.H. Lee, J.S. Jang, N.K. Chung, C.Y. Park, U.B.

Baek, et al., Characterization technique of gases permeation properties in polymers: H_2, He, N_2 and Ar gas, Sci. Rep. 12 (2022) 3328.
[39] J.H. Lee, Y.W. Kim, N.K. Chung, H.M. Kang, W.J. Moon, M.C. Choi, et al., Multiphase modeling of pressure-dependent hydrogen diffusivity in fractal porous structures of acrylonitrile butadiene rubber-carbon black composites with different fillers, Polymer 311 (2024) 127552.
[40] C.H. Lee, J.K. Jung, K.S. Kim, C.J. Kim, Hierarchical channel morphology in O-rings after two cycling exposures to 70 MPa hydrogen gas: a case study of sealing failure, Sci. Rep. 14 (2024) 5319.
[41] Y. Moon, H. Lee, J. Jung, H. Han, Direct visualization of carbon black aggregates in nitrile butadiene rubber by THz near-field microscope, Sci. Rep. 13 (2023) 7846.
[42] J.K. Jung, C.H. Lee, U.B. Baek, M.C. Choi, J.W. Bae, Filler influence on H_2 permeation properties in sulfur-crosslinked ethylene propylene diene monomer polymers blended with different concentrations of carbon black and silica fillers, Polymers 14 (2022) 592.
[43] G.H. Kim, Y.I. Moon, J.K. Jung, M.C. Choi, J.W. Bae, Influence of carbon black and silica fillers with different concentrations on dielectric relaxation in nitrile butadiene rubber investigated by impedance spectroscopy, Polymers 14 (2022) 155.
[44] C. Liu, R. Zhang, L. Tian, Y. Pei, Y. Li, Research progress on compatibility of non-metallic pipes in hydrogen environment, Nat. Gas Ind. 42 (2022) 145–156.
[45] D.B. Smith, B.J. Frame, L.M. Anovitz, C. Makselon, Feasibility of using glass-fiber-reinforced polymer pipelines for hydrogen delivery, Proceedings of the ASME 2016 Pressure Vessels and Piping Conference, Vancouver, Canada, 2016, pp. 17–21.
[46] S. Tanaka, A. Higashitani, K. Sugie, M. Esashi, Hydrogen supply using borohydride and prototyping of a miniature fuel cell by sand blasting, IEEJ Trans. Sens. Micromachines 123 (2003) 340–345.
[47] J. Le Pree, Strengthening the weakest link, Chem. Eng. 116 (2009) 19.
[48] B. Brushan, D.F. Wilcock, Wear behavior of polymeric compositions in dry reciprocating sliding, Wear 75 (1982) 41–70.
[49] S. Yuan, S. Zhang, J. Wei, Y. Gao, Y. Zhu, H. Wang, Materials selection, design, and regulation of polymer-based hydrogen barrier composite coatings, membranes and films for effective hydrogen storage and transportation: A comprehensive review, Int. J. Hydrogen Energy 91 (2024) 555–573.
[50] G. Li, J. Zhang, J. Chai, Z. Ni, Y. Yan, Cryogenic mechanical performance and gas-barrier property of epoxy resins modified with multi-walled carbon nanotubes, Int. J. Hydrogen Energy 89 (2024) 738–745.
[51] P.S. Chauhan, G. Bhatt, S. Bhattacharya, Leakage monitoring in inflatable space antennas: a perspective to sensitive detection of helium and nitrogen gases, in: S. Bhattacharya, A. Agarwal, O. Prakash, S. Singh (Eds), Energy, Environment, and Sustainability, Springer, Singapore, 2018, pp. 209–222.
[52] H. Itou, S. Tsurumaki, T. Moriga, A. Yamada, G. Inoue, Y. Matsukuma, et al., Study on deterioration mechanism of polymer electrolyte fuel cell, kagaku kogaku ronbunshu 35 (2009) 184–190.
[53] J.K. Jung, K.T. Kim, J.H. Lee, U.B. Baek, Effective and low-cost gas sensor based on a light intensity analysis of a webcam image: Gas enriched polymers under high pressure, Sens. Actuators B Chem. 393 (2023) 134258.
[54] J. Jung, G. Kim, G. Gim, C. Park, J. Lee, Determination of gas permeation properties in polymer using capacitive electrode sensors, Sensors 22 (2022) 1141.
[55] Y. Nishijima, A. Balčytis, G. Seniutinas, S. Juodkazis, T. Arakawa, S. Okazaki, et al., Plasmonic hydrogen sensor at infrared wavelengths, Sens. Mater. 29 (2017) 1269–1274.
[56] V. Kumar, R. Sakla, N. Sharma, Kanika, R. Khan, D.A. Jose, Liposome Based Near-Infrared Sensors for the Selective Detection of Hydrogen Sulfide, ChemPlusChem 88 (2023) e202300243.
[57] A. Ji, Y. Fan, W. Ren, S. Zhang, H.-W. Ai, A sensitive near-infrared fluorescent sensor for mitochondrial hydrogen sulfide, ACS Sens. 3 (2018) 992–997.
[58] J.F. da Silveira Petruci, P.R. Fortes, V. Kokoric, A. Wilk, I.M. Raimundo, A.A. Cardoso, et al., Monitoring of hydrogen sulfide via substrate-integrated hollow waveguide mid-infrared sensors in real-time, Analyst 139 (2014) 198–203.
[59] X. L. Yu, F. Li, L.H. Chen, X.Y. Chang, A compact sensor based on near infrared absorption spectroscopy for flow diagnostics in a low density hydrogen and oxygen combustion driven shock tube, Lasers Eng. 23 (2012) 1–17.
[60] G. Li, K. Ma, Y. Jiao, X. Zhang, Z. Zhang, Y. Wu, et al., A near-infrared trace hydrogen sulfide sensor based on CEEMDAN and PSO-LSSVM, Microw. Opt. Technol. Lett. 65 (2021) 1047–1053.
[61] Q. Ma, L. Li, Z. Gao, S. Tian, J. Yu, X. Du, et al., Near-infrared sensitive differential Helmholtz-based hydrogen sulfide photoacoustic sensors, Opt. Express 31 (2023) 14851–14861.
[62] D. Liu, G. Chen, G. Fang, A near-infrared, colorimetric and ratiometric fluorescent sensor with high sensitivity to hydrogen peroxide and viscosity for solutions detection and imaging living cells, Bioorg. Chem. 119 (2022) 105513.
[63] J. Kübel, G. Lee, S.A. Ooi, S. Westenhoff, H. Han, M. Cho, M. Maj, Ultrafast chemical exchange dynamics of hydrogen bonds observed via isonitrile infrared sensors: implications for biomolecular studies, J. Phys. Chem. Lett. 10 (2019) 7878–7883.
[64] L. Gao, Y. Tian, A. Hussain, Y. Guan, G. Xu, Recent developments and challenges in resistance-based hydrogen gas sensors based on metal oxide semiconductors, Anal. Bioanal. Chem. 416 (2024) 3697–3715.
[65] R. Werner, P. Prosposito, A. Böhme, A.H. Foitzik, Micro structured, multipurpose hydrogen alarm sensor system on semiconductor basis, in: R. Montanari, M. Richetta, M. Febbi, E. M. Staderini (Eds.), Mechanisms and Machine Science, Springer Nature, Switzerland, 2024, pp. 190–197.
[66] A. Alaghmandfard, S. Fardindoost, A.L. Frencken, M. Hoorfar, The next generation of hydrogen gas sensors based on transition metal dichalcogenide-metal oxide semiconductor hybrid structures, Ceram. Int. 50 (2024) 29026–29043.

[67] V. Kafil, B. Sreenan, M. Hadj-Nacer, Y. Wang, J. Yoon, M. Greiner, et al., Review of noble metal and metal-oxide-semiconductor based chemiresistive hydrogen sensors, Sens. Actuators A Phys. 373 (2024) 115440.
[68] R.M. Aljarrah, R.A. Nawar, Enhance hydrogen sulfide (H_2S) gas sensor based on metal oxide semiconductor (NiO) thin films, Iran. J. Phys. Res. 23 (2023) 59–65.
[69] W. Li, R. Sokolovskij, H. Zheng, J. He, M. He, Q. Wang, et al., Low concentration hydrogen detection properties of metal-insulator-semiconductor AlGaN/GaN HEMT sensor, Sens. Actuators B Chem. 392 (2023) 134050.
[70] S. Ghosh, L. Rajan, II-VI Semiconductor-based Thin-Film Transistor Sensor for Room Temperature Hydrogen Detection From Idea to Product Development, in: G. Rawat, A.B. Yadav (Eds.), Nanoelectronics devices: Design, materials, and applications (Part I), Bentham Science Publishers, Sharjah, 2023, pp. 182–207.
[71] N.P. Maksymovych, G.V. Fedorenko, L.P. Oleksenko, Nanosized Pd/SnO2 materials for semiconductor hydrogen sensors, Theor. Exp. Chem. 58 (2022) 247–253.
[72] K.M.B. Urs, K. Sahoo, N. Bhat, V. Kamble, Complementary metal oxide semiconductor-compatible top-down fabrication of a Ni/NiO nanobeam room temperature hydrogen sensor device, ACS Appl. Electron. Mater. 4 (2022) 87–91.
[73] J.K. Jung, I.G. Kim, K.T. Kim, U.B. Baek, S.H. Nahm, Novel volumetric analysis technique for characterizing the solubility and diffusivity of hydrogen in rubbers, Curr. Appl. Phys. 26 (2021) 9–15.
[74] T. Sahoo, P. Kale, Work function-based metal–oxide–semiconductor hydrogen sensor and its functionality: A review, Adv. Mater. Interfaces 8 (2021) 2100649.
[75] C. Schultealbert, J. Amann, T. Baur, A. Schütze, Measuring hydrogen in indoor air with a selective metal oxide semiconductor sensor, Atmosphere 12 (2021) 366.
[76] D.D.O. Henriquez, I. Cho, H. Yang, J. Choi, M. Kang, K.S. Chang, et al., Pt nanostructures fabricated by local hydrothermal synthesis for low-power catalytic-combustion hydrogen sensors, ACS Appl. Nano Mater. 4 (2021) 7–12.
[77] W. Jang, J.S. Park, K.W. Lee, Y. Roh, Methane and hydrogen sensing properties of catalytic combustion type single-chip micro gas sensors with two different Pt film thicknesses for heaters, Micro Nano Syst. Lett. 6 (2018) 7.
[78] H. Oigawa, M. Shimojima, T. Tsuno, T. Ueda, Stable heating technology for catalytic combustion hydrogen gas sensor using quartz resonators, Sens. Mater. 30 (2018) 1103–1114.
[79] X. Liu, H. Dong, S. Xia, Micromachined catalytic combustion type gas sensor for hydrogen detection, Micro Nano Lett. 8 (2013) 668–671.
[80] M. Yuasa, T. Nagano, N. Tachibana, T. Kida, K. Shimanoe, Catalytic combustion-type hydrogen sensor using BaTiO3-based PTC thermistor, J. Am. Ceram. Soc. 96 (2013) 1789–1794.
[81] C.-H. Han, D.-W. Hong, S.-D. Han, J. Gwak, K.C. Singh, Catalytic combustion type hydrogen gas sensor using TiO2 and UV-LED, Sens. Actuators B Chem. 125 (2007) 224–228.
[82] M. Krawczyk, J. Namiesnik, Application of a catalytic combustion sensor (Pellistor) for the monitoring of the explosiveness of a hydrogen-air mixture in the upper explosive limit range, J. Autom. Methods Chem. 25 (2003) 115–122.
[83] H. Bao, W. Jin, Y. Miao, Optical fiber hydrogen sensor with stimulated Raman dispersion spectroscopy, Proceedings of the 26th International Conference on Optical Fiber Sensors, Lausanne, Switzerland, 2018.
[84] M. Basso, V. Paolucci, V. Ricci, E. Colusso, M. Cattelan, E. Napolitani, et al., Sol-Gel Pt-VO2 films as selective chemoresistive and optical H_2 gas sensors, ACS Appl. Mater. Interfaces 16 (2024) 57558–57570.
[85] M. Zhou, X. Liu, R. Cui, L. Dong, H. Wu, Detection of hydrogen sulfide gas in sewer based on light-induced thermoelastic spectroscopy, Laser Optoelectron. Prog. 61 (2024) 0330002.
[86] S. Yao, M. Zhang, H. Gao, Y. Zhang, J. Liu, Y. Yang, X. Wang, Development of four-channel hydrogen sensor based on stimulate Raman spectroscopy, Proceedings of AOPC 2023: Optic Fiber Gyro, Beijing, China, 2023, pp. 554–558.
[87] T. Liang, S. Qiao, X. Liu, Y. Ma, Highly sensitive hydrogen sensing based on tunable diode laser absorption spectroscopy with a 2.1 μm diode laser, Chemosensors 10 (2022) 321.
[88] J.K. Jung, K.T. Kim, N.K. Chung, U.B. Baek, S.H. Nahm, Characterizing the Diffusion Property of Hydrogen Sorption and Desorption Processes in Several Spherical-Shaped Polymers, Polymers14 (2022) 1468.
[89] Z. Weiss, J. Čapek, Z. Kačenka, O. Ekrt, J. Kopeček, M. Losertová, D. Vojtěch, Analysis of hydrogen in a hydrogenated, 3D-printed Ti–6Al–4V alloy by glow discharge optical emission spectroscopy: sample heating effects, J. Anal. At. Spectrom. 39 (2024) 996–1003.
[90] D. Bizyaev, The neutral hydrogen mass in galaxies estimated via optical spectroscopy, Mon. Not. R. Astron. Soc. Lett. 528 (2024) L146–L151.
[91] M. Mazzaglia, L. Celona, S. Gammino, G. Torrisi, D. Mascali, Optical emission spectroscopy measurements of hydrogen and argon plasmas at high resolution, Nuovo Cimento Soc. Ital. Fis. C 44 (2021) 58.
[92] C. Lee, N. Leconte, J. Kim, D. Cho, I.-W. Lyo, E.J. Choi, Optical spectroscopy study on the effect of hydrogen adsorption on graphene, Carbon 103 (2016) 109–114.
[93] H. Takahara, R. Ishigami, K. Kodama, A. Kojyo, T. Nakamura, Y. Oka, Hydrogen analysis in diamond-like carbon by glow discharge optical emission spectroscopy, J. Anal. At. Spectrom. 31 (2016) 940–947.
[94] M. Curioni, F. Scenini, T. Monetta, F. Bellucci, Investigation of hydrogen evolution behaviour on corroding magnesium electrodes by electrochemical impedance spectroscopy, real-Time hydrogen measurement and optical imaging, Eur. Corros. Congr. 2 (2015) 1005.
[95] N.S. Pushilina, V.N. Kudiiarov, A.N. Nikolaeva, Investigation of hydrogen distribution in zirconium alloy by means glow discharge optical emission spectroscopy, Proceedings of 2014 9th International Forum on Strategic Technology (IFOST), Cox's Bazar, Bangladesh, 2014, pp. 489–491.
[96] A.M. Lider, N.S. Pushilina, V.N. Kudiiarov, M. Kroening,

Investigation of hydrogen distribution from the surface to the depth in technically pure titanium alloy with the help of glow discharge optical emission spectroscopy, Appl. Mech. Mater. 302 (2013) 92–96.
[97] E.D. Gaspera, M. Bersani, G. Mattei, T.L. Nguyen, P. Mulvaney, A. Martucci, Cooperative effect of Au and Pt inside TiO2 matrix for optical hydrogen detection at room temperature using surface plasmon spectroscopy, Nanoscale 4 (2012) 5972–5979.
[98] C. Noguez, C. Beitia, W. Preyss, A.I. Shkrebtii, M. Roy, Y. Borensztein, R. Del Sole, Theoretical and experimental optical spectroscopy study of hydrogen adsorption at Si(111)−(7×7), Phys. Rev. Lett. 76 (1996) 4923.
[99] A. Hinojo, E. Lujan, J. Abella, S. Colominas, Development and characterization of electrochemical hydrogen sensors using different fabrication techniques, Fusion Eng. Des. 204 (2024) 114483.
[100] W.M. Seleka, K.E. Ramohlola, K.D. Modibane, E. Makhado, Conductive chitosan/polyaniline hydrogel: a gas sensor for room-temperature electrochemical hydrogen sensing, Int. J. Hydrog. Energy 68 (2024) 940–954.
[101] D. Yadav, A. Shrivastava, A. Sircar, P. Dhorajiya, A. Muniya, R.P. Bhattacharyay, Development and performance evaluation of Sr2CeO4 - SrCe0.85Y0.15O3-ϖ based electrochemical hydrogen isotopes sensor, Fusion Eng. Des. 200 (2024) 114189.
[102] Y. Ha, J. Kwon, S. Choi, D. Jung, Fabrication of Pt/Carbon nanotube composite based electrochemical hydrogen sulfide gas sensor using 3D printing, J. Sens. Sci. Technol. 32 (2023) 290–294.
[103] C. Wang, J. Yang, J. Li, C. Luo, X. Xu, F. Qian, Solid-state electrochemical hydrogen sensors: a review, Int. J. Hydrog. Energy 48 (2023) 31377–31391.
[104] A. Hinojo, E. Lujan, M. Nel-lo, S. Colominas, J. Abella, BaCe0.6Zr0.3Y0.1O3-α electrochemical hydrogen sensor for fusion applications, Fusion Eng. Des. 188 (2023) 113452.
[105] E. Gorbova, G. Balkourani, C. Molochas, D. Sidiropoulos, A. Brouzgou, A. Demin, et al., Brief review on high-temperature electrochemical hydrogen sensors, Catalysts 12 (2022) 1647.
[106] F. Shi, J. Geng, B. Ara, B. Wang, X. Li, Q. Ma, et al., Flexible electrochemical sensor based on N-doped helical carbon nanotubes coated manganese oxide nanoparticles for real-time monitoring of cellular hydrogen peroxide release, Microchem. J. 207 (2024) 112194.
[107] E.G. Lee, S.W. Jung, Y.E. Jo, H.R. Yoon, B.K. Yoo, S.H. Choi, et al., Electrochemical hydrogen sensor assembly for monitoring high-concentration hydrogen, Phys. Status Solidi (a) 219 (2022) 2100782.
[108] E. Isik, L. B. Tasyurek, I. Isik, N. Kilinc, Synthesis and analysis of TiO2 nanotubes by electrochemical anodization and machine learning method for hydrogen sensors, Microelectron. Eng. 262 (2022) 111834.
[109] A.S. Kalyakin, D.A. Medvedev, A.N. Volkov, Electrochemical zirconia-based sensor for measuring hydrogen diffusion in inert gases, J. Electrochem. Soc. 169 (2022) 057530.
[110] N. Holstein, W. Krauss, F. S. Nitti, Detection of hydrogen as impurity in liquid lithium: An electrochemical hydrogen-sensor for IFMIF-DONES, Fusion Eng. Des. 178 (2022) 113085.
[111] N.S. Dumore, M. Mukhopadhyay, Sensitivity enhanced SeNPs-FTO electrochemical sensor for hydrogen peroxide detection, J. Electroanal. Chem. 878 (2020) 114544.
[112] A. Juárez Hernández, G. Trapaga-Martinez, J.L. Camacho-Martinez, C. Gonzalez-Rivera, I.L. Juarez, Alternative system to measure hydrogen content in molten aluminium using an electrochemical sensor, Indian J. Eng. Mater. Sci. 27 (2021) 1037–1042.
[113] S.H. Kim, D.K. Han, S.Hong, B.R. Jeong, B.S. Park, S.D. Han, et al., Quasi-solid-state hybrid electrolytes for electrochemical hydrogen gas sensor, J. Electrochem. Sci. Technol. 10 (2019) 294–301.
[114] N. Holstein, W. Krauss, J. Konys, F.S. Nitti, Development of an electrochemical sensor for hydrogen detection in liquid lithium for IFMIF-DONES, Fusion Eng. Des. 146 (2019) 1441–1445.
[115] A. Ruchets, N. Donker, D. Schönauer-Kamin, R. Moos, J. Zosel, U. Guth, M. Mertig, Selectivity improvement towards hydrogen and oxygen of solid electrolyte sensors by dynamic electrochemical methods, Sens. Actuators B Chem. 290 (2019) 53–58.
[116] J.K. Jung, I.G. Kim, K.S. Chung, Y.I. Kim, D.H. Kim, Determination of permeation properties of hydrogen gas in sealing rubbers using thermal desorption analysis gas chromatography, Sci. Rep. 11 (2021) 17092.
[117] J.K. Jung, I.G. Kim, K.S. Chung, U.B. Baek, Gas chromatography techniques to evaluate the hydrogen permeation characteristics in rubber: ethylene propylene diene monomer, Sci. Rep. 11 (2021) 4859.
[118] J.K. Jung, K.T. Kim, K.S. Chung, Two volumetric techniques for determining the transport properties of hydrogen gas in polymer, Mater. Chem. Phys. 276 (2022) 125364.
[119] J.K. Jung, I.G. Kim, K.T. Kim, K.S. Ryu, K.S. Chung, Evaluation techniques of hydrogen permeation in sealing rubber materials, Polym. Test. 93 (2021) 107016.
[120] L. Yang, Q. Han, S. Cao, F. Huang, M. Qin, C. Guo, M. Ding, Research on the interaction of hydrogen-bond acidic polymer sensitive sensor materials with chemical warfare agents simulants by inverse gas chromatography, Sensors 15 (2015) 12884–12890.
[121] K.W. Lou, C.L. Ho, Y.P. Ho, Gas chromatography system with a modular gas sensor for the regeneration of sensor sensitivity, Proceedings of 2023 IEEE 16th International Conference on Nano/Molecular Medicine & Engineering (NANOMED), Okinawa, Japan, 2023, pp. 194–198.
[122] D. Kumar, V. Kumar, A. Sachdev, I. Matai, Electrochemical microfluidic sensor based on hBN-CeO2@Cyt c hydrogel-modified SPCE for the detection of hydrogen peroxide, Ionics 30 (2024) 8559–8575.
[123] Z. Huang, W. Yang, Y. Zhang, J. Yin, X. Sun, J. Sun, et al., Miniaturized electrochemical gas sensor with a functional nanocomposite and thin ionic liquid interface for highly sensitive and rapid detection of hydrogen, Anal. Chem. 96 (2024) 17960–17968.
[124] J. Yin, H. Zhang, Y. Wang, M.B.J. Laurindo, J. Zhao, Y.

Hasebe, et al., Crab gill–derived nanorod-like carbons as bifunctional electrochemical sensors for detection of hydrogen peroxide and glucose, Ionics 30 (2024) 3541–3552.
[125] M. Doering, L.L. Trinkies, J. Kieninger, M. Kraut, S.J. Rupitsch, R. Dittmeyer, et al., In situ performance monitoring of electrochemical oxygen and hydrogen peroxide sensors in an additively manufactured modular microreactor, ACS Omega 9 (2024) 19700–19711.
[126] H. Wang, Y. Li, L. Tian, X. Li, Q. Gao, Y. Liu, et al., A LAMP-based hydrogen ion selective electrochemical sensor for highly sensitive detection of Mycoplasma pneumoniae, Anal. Methods 16 (2024) 3020–3029.
[127] H. Liu, Y. Yu, T. Xue, C. Gan, Y. Xie, D. Wang, et al., A nonenzymatic electrochemical sensor for the detection of hydrogen peroxide in vitro and in vivo fibrosis models, Chin. Chem. Lett. 35 (2024) 108574.
[128] J.K. Jung, I.G. Kim, S.K. Jeon, K.S. Chung, Characterizing the hydrogen transport properties of rubbery polymers by gravimetric analysis, Rubber Chem. Technol. 94 (2021) 688–703.
[129] X. Zhu, W. Ahmed, K. Schmidt, R. Barroso, S.J. Fowler, C.F. Blanford, Validation of an electronic VOC sensor against gas chromatography–mass spectrometry, IEEE Trans. Instrum. Meas. 73 (2024) 1–8.
[130] B.H.R. Varma, B.S. Rao, Gas chromatography-head space-mass spectrometry sensor based quality control of dobutamine hydrochloride bulk material for a mutagenic impurity, 2-bromopropane, Res. J. Chem. Environ. 27 (2023) 54–61.
[131] S. Löbbecke, A. Pape, L. Montero, F. Uteschil, J.F. Ayala-Cabrera, O.J. Schmitz, Improving the reliability of phthalate esters analysis in water samples by gas chromatography-tube plasma ionization-high-resolution mass spectrometry (GC-TPI-HRMS), Talanta 285 (2025) 127388.
[132] J. Kwon, H. Kim, M.Z. Siddiqui, H.-S. Kang, J.-H. Choi, S. Kumagai, et al., A comprehensive pyrolysis-gas chromatography/mass spectrometry analysis for the assessment of microplastics in various salts, Food Chem. 467 (2025) 142193.
[133] R. Meng, D. Pu, Z. Xu, J. Liu, Q. Zhang, M. Xu, et al., Decoding the aroma changes of stir-fried shredded potatoes with different soy sauces using thermal desorption combined with gas chromatography–mass spectrometry and sensory evaluation, Food Chem. 467 (2025) 142252.
[134] P. Li, S. Li, W. Zhao, A. Zhang, J. Liu, Y. Wang, et al., Characteristic odor of foxtail millet from different area with different sowing time based on gas chromatography-mass spectrometry, J. Future Foods 5 (2025) 50–56.
[135] P.D. Zander, F. Rubach, A. Martínez-García, Large-volume injection and assessment of reference standards for n-alkane δD and δ(13)C analysis via gas chromatography isotope ratio mass spectrometry, Rapid Commun. Mass Spectrom. 39 (2025) e9943.
[136] X. He, H.H. Jeleń, Comprehensive two dimensional gas chromatography – time of flight mass spectrometry (GC×GC-TOFMS) for the investigation of botanical origin of raw spirits, Food Chem. 465 (2025) 142004.
[137] G. Feng, J. Li, J. Liu, R. Tan, Examining the effects of processing techniques on the quality of hawk tea through liquid chromatography–tandem mass spectrometry and two-dimensional gas chromatography–time-of-flight mass spectrometry, Food Chem. 465 (2025) 142012.
[138] B. Quintanilla-Casas, B. Torres-Cobos, R. Bro, F. Guardiola, S. Vichi, A. Tres, The volatile metabolome — gas chromatography–mass spectrometry approaches in the context of food fraud, Curr. Opin. Food Sci. 61 (2024) 101235.
[139] J. Hao, F. Xu, D. Yang, B. Wang, Y. Qiao, Y. Tian, Analytical pyrolysis of biomass using pyrolysis-gas chromatography/mass spectrometry, Renew. Sustain. Energy Rev. 208 (2025) 115090.
[140] J. Steff, M.K. Parr, Same, but different: Variations in fragment ions among stereoisomers of a 17α-methyl steroid in gas chromatography/electron ionization mass spectrometry, Rapid Commun. Mass Spectrom. 39 (2025) e9934.
[141] J.H. Lee, J.K. Jung, Development of image-based water level sensor with high-resolution and low-cost using image processing algorithm: application to outgassing measurements from gas-enriched polymer, Sensors 24 (2024) 7699.
[142] J.K. Jung, I.G. Kim, S.K. Jeon, K.-T. Kim, U.B. Baek, S.H. Nahm, Volumetric analysis technique for analyzing the transport properties of hydrogen gas in cylindrical-shaped rubbery polymers, Polym. Test. 99 (2021) 107147.
[143] J.K. Jung, J.H. Lee, S.K. Jeon, N.H. Tak, N.K. Chung, U.B. Baek, et al., Correlations between H_2 permeation and physical/mechanical properties in ethylene propylene diene monomer polymers blended with carbon black and silica fillers, Int. J. Mol. Sci. 24 (2023) 2865.
[144] J.K. Jung, K.T. Kim, U.B. Baek, Simultaneous three-channel measurements of hydrogen diffusion with light intensity analysis of images by employing webcam, Curr. Appl. Phys. 37 (2022) 19–26.
[145] J.K. Jung, Review of developed methods for measuring gas uptake and diffusivity in polymers enriched by pure gas under high pressure, Polymers 16 (2024) 723.
[146] J. Crank, The Mathematics of Diffusion, Oxford, Clarendon Press, 1979.
[147] A. Demarez, A.G. Hock, F.A. Meunier, Diffusion of hydrogen in mild steel, Acta Metall. 2 (1954) 214–223.
[148] J.A. Nelder, R. Mead, A simplex method for function minimization, Comput. J. 7 (1965) 308–313.
[149] J.K. Jung, J.H. Lee, Y.W. Kim, N.K. Chung, Development of portable gas sensing system for measuring gas emission concentration and diffusivity using commercial manometric sensors in gas charged polymers: Application to pure gases, H_2, He, N_2, O_2 and Ar, Sens. Actuators B Chem. 418 (2024) 136240.
[150] J.K. Jung, C.H. Lee, M.S. Son, J.H. Lee, U.B. Baek, K.S. Chung, et al., Filler effects on H_2 diffusion behavior in nitrile butadiene rubber blended with carbon black and silica fillers of different concentrations, Polymers 14 (2022) 700.
[151] J.K. Jung, K.T. Kim, U.B. Baek, S.H. Nahm, Volume dependence of hydrogen diffusion for sorption and desorption processes in cylindrical-shaped polymers, Polymers 14 (2022) 756.